PCCP

Accepted Manuscript

A facile one-pot synthesis of blue and red luminescent thiol stabilized gold nanocluster: a thorough optical and microscopy study

Nabin Kumar Pal, Carola Kryschi*
Department of Chemistry and Pharmacy and ICMM, Friedrich-Alexander-University of Erlangen-Nuremberg, Erlangen, Germany.
*Email: carola.kryschi@fau.de

Abstract

Here in this contribution, blue and red luminescent 1-dodecanethiol (DT) terminated gold nanocluster (AuNC) were prepared by a simple two-step synthesis route where the first step involved the surfactant-free synthesis of bare AuNC in N,N´-dimethylformamide (DMF) and the second step is the termination of the as-prepared bare AuNC by 1-dodecanethiol. The blue and red luminescent DT-terminated AuNC were isolated by a solvent-induced precipitation followed by ultra-centrifugation technique. Both, the bare AuNC and the blue and red luminescent DT-terminated AuNC exhibit stable photoluminescence and good solubility in various solvents. The photo-physical, electronic, structural, and morphological properties of the bare AuNC and the blue and red luminescent DT-terminated AuNC were examined by performing UV-Vis absorption spectroscopy, stationary and time-resolved PL spectroscopy, X-ray photoelectron spectroscopy (XPS), femtosecond transient absorption spectroscopy, Fourier-Transform infrared spectroscopy (FTIR-ATR), and high-resolution transmission electron microscopy (HRTEM) experiments.

1. Introduction

Over the past two decades, few-atoms sub-nanometer sized, noble metal nanocluster have gained tremendous significance in both, material and biological science[1-3]. Owing to their existence, as a missing link between atoms and nanocrystals, these nanocluster exhibit wide ranges of new material properties such as shape- and size-tunable optical, electronic, and electrical properties, molecular-like properties such as quantized charging, discrete energy states and size-dependent photoluminescence[4,5]. These novel properties along with low toxicity and good biocompatibility make these nanocluster an important entity for researchers and make them feasible for applications in catalysis[6], optical sensing[7], bio-imaging[8], single molecule-optoelectronics[9] and surface-enhanced Raman spectroscopy[10].

The use of thiols as a protecting agent for the synthesis of gold nanocluster is well established. The reason for this is mainly because of the formation of covalent bonds at gold surface via sulphur head group. The synthesis of thiol-derivatized stable gold nanoparticles was first reported by Brust and Schiffrin in the mids of 1990[11]. Following this seminal work, various methods have been developed so far to synthesize monodisperse gold nanocluster of definite particle sizes by controlling the initial reaction conditions such as thiol-to-gold ion ratio, reducing agents, temperature and also by modifying the post-synthetic purification processes. Several well defined nanoclusters have been synthesized so far such as $Au_{20}(SR)_{16}$, $Au_{25}(SR)_{18}$, $Au_{38}(SR)_{24}$, $Au_{102}(SR)_{44,}$ and $Au_{144}(SR)_{60}$ [12-17]. Among all these thiolate protected gold nanocluster, $Au_{25}(SR)_{18}$ and $Au_{144}(SR)_{60}$ are most widely studied due to their higher stability in comparison to other thiolated gold nanoclusters. The X-ray crystal structure of $Au_{25}(SCH_2CH_2Ph)_{18}$ nanocluster was also recently determined in both, anionic and neutral forms [18]. All these nanoclusters were synthesized by using a thiol as a protecting ligand in an organic solvent. The use of organic solvents as a reaction medium makes these nanoclusters soluble only in organic solvents. However, water solubility of the nanocluster is very crucial for biological applications (*e.g.* biological imaging, labelling and therapeutics). Several reports are available where gold nanocluster were prepared using proteins[19], dendrimers[20], amino acids[21], DNA[22] and polyelectrolytes[23] as scaffolds. However, most of the methods mentioned above need an expensive starting material, photo-irradiation, electric field application or an external toxic reducing agent such as sodium borohydride. The synthesis of noble metal nanocluster without the use of external reducing agents was demonstrated in recent past by Liz-Marzán and co-workers using N,N′-dimethylformamide (DMF) as both, mild reducing and stabilizing agent[24]. However, they only succeeded in producing non-luminescent nanoparticles with sizes larger than 5 nm. These noble metal nanoparticles exhibit intense surface plasmon bands in the UV-Vis absorption spectrum. Later Liu et al.[25] extended this idea of using DMF as both, reducing and stabilizing agent at high temperature and they have succeeded in developing a surfactant-free recipe to synthesize highly stable and luminescent gold nanocluster. Recently, Yabu et al.[26] reported of a novel one-pot process for the synthesis of AuNC via simple reduction of Au ions by amino-terminated poly (1,2-butadiene) ($PB-NH_2$) in toluene. The synthesized AuNC show PL-emission at 465 nm upon excitation at 370 nm and were characterized as Au_8 clusters (from MALDI-TOF MS analysis).

In this contribution we refer to a surfactant-free synthesis route to prepare highly stable and blue luminescent AuNC using N,N-dimethylformamide (DMF) as both, reducing and protecting agent, following the method originally proposed by Liu et al.[25] with minor modifications. The as-synthesized bare AuNC were terminated with 1-dodecanethiol (1-DT). Moreover, here we demonstrated for the first time that the long-time aging reaction between bare AuNC and an excess of 1-DT produces both, blue and red luminescent DT-terminated AuNC in the same pot. These two differently sized nanocluster were separated very conveniently through a solvent-induced precipitation method followed by ultracentrifugation. Both, blue and red luminescent DT-terminated gold nanocluster were readily dissolved in methanol and water for further characterizations.

2. Experimental parts

2.1 Materials

Hydrogen tetrachloroaurate (III) trihydrate ($HAuCl_4.3H_2O$, ≥ 99.5 %, p.a), $NaBH_4$ (97 %) and N, N´-dimethylformamide (≥ 99.8 %) were purchased from Roth, 1-dodecanethiol (DT, 99 %) and methanol (anhydrous, 99.8 %) were obtained from Aldrich. All materials and solvents were used as received from the suppliers without further purification. In all synthesis milli-Q de-ionised water (18 MΩ) was used.

2.2 Synthesis of uncoated-gold nanocluster (AuNC)

The bare AuNC were prepared according to the DMF reduction technique that was previously reported by Liu et al[25]. In a typical procedure, 30 ml of N, N'-dimethylformamide (DMF) was poured in to a three neck round-bottom flask under argon atmosphere. The flask was then slowly heated in a silicon-oil bath and kept as such until the temperature reaches 145°C. A solution of 300 µl of 0.1 M aqueous $HAuCl_4$ was then added to this pre-heated DMF solution at once under vigorous stirring. The reaction was allowed to proceed for 6 h under reflux. After 6 h of refluxing a light yellow-coloured solution was obtained that was centrifuged thrice at 12000 rpm for 30 min, in order to remove the larger gold nanoparticles and other impurities. After centrifugation the solution was evaporated under high vacuum to remove the excess solvent. The residue thus obtained was dissolved in methanol for further characterizations and functionalization.

2.3 Functionalization of the as-prepared bare AuNC with 1-dodecanethiol (DT)

To 3 ml of the methanolic solution of the as-prepared AuNC, 0.1 mmol of 1-dodecanethiol (ligand-to-AuNC mole ratio ≈ 3) was added under vigorous stirring. The reaction was allowed to proceed in the dark for about 24 h. After the completion of the ligand binding process the solution was aged for another 24 h. During this aging process some of the initially formed blue luminescent DT-terminated AuNC start to grow to larger red luminescent AuNC. Finally 5 ml of de-ionised water was added which was followed by centrifugation at 12000 rpm for 30 min to separate the blue and red luminescent DT-terminated AuNC. The red luminescent AuNC were obtained in the precipitate, whereas the blue luminescent AuNC remain in the solution. Both these DT-terminated AuNC were dissolved in methanol for further characterizations.

3. Methods and instrumentations

3.1 High-Resolution Transmission Electron Microscopy (HRTEM)

The HRTEM images were recorded using a Phillips CM 300 UltraTwin microscope. The measurements were carried out at an accelerating voltage of 300 kV in the bright-field mode. The samples for HRTEM were prepared by dropcasting 5 microliter of the ethanolic solution of the DT-terminated blue and red luminescent AuNC onto an ultrathin carbon coated copper grid (300 mesh) followed by drying in a vacuum at 25°C for 2 days.

3.2 X-ray Photoelectron Spectroscopy

The chemical compositions of the bare AuNC were investigated with X-ray photoelectron spectroscopy (XPS, PHI 5600 XPS spectrometer). Monochromatic Al K_α was used as the X-ray source.

3.3 Fourier-Transform Infrared Spectroscopy-Attenuated Total reflection (FTIR-ATR)

The infrared spectrum were taken in the attenuated total reflection mode (ATR) using a FTIR-spectrometer (Prestige-21 Shimadzu) equipped with a smart-orbit ATR attachment containing a single reflection diamond crystal. The angle of incidence relative to the ATR crystal surface was 45° in the analysis. Typically 100 scans were performed with a 4 cm^{-1} resolution.

3.4 Steady-State Optical Spectroscopy

The PL spectra were recorded on a Jobin-Yvon FluoroMax-3 spectrofluorometer using the magic-angle polarization configuration and a slit width of 5 nm for both excitation and emission spectra. The UV-Vis absorption spectra were recorded on a Perkin Elmer UV-Vis absorption spectrometer Lambda 2. All experiments were performed at room temperature using quartz cuvettes with an optical path length of 10 mm. The PL quantum yields of the DT-terminated blue- and red-luminescent AuNC were estimated using a fluorescence standard. The following relative comparison method was used to evaluate the quantum yield:

$$\frac{Q_t}{Q_s} = \frac{(I_t / A_t)\eta_t^2}{(I_s / A_s)\eta_s^2} \qquad (1)$$

where Q is the PL quantum yield, I the integral area under the PL spectrum, η the refractive index of the solvent, and A the absorption at the selected excitation wavelength. The subscripts “t” and “s” represent the test sample and fluorescence standard, respectively.

3.5 Time-Resolved Optical Spectroscopy

PL decay profiles were recorded using the time-correlated single-photon counting (TCSPC) PL spectroscopy technique. This time resolved measurement of the PL intensity was carried out on the TCSPC spectrometer Fluorolog-3 (Jobin Yvon) equipped with a microchannel plate (Hamamatsu, R3809U-50) that provides a time resolution of about 60 ps.

Femtosecond transient absorption spectroscopy experiments were conducted with a Clark MXR CPA 2101 laser system in conjunction with an Ultrafast TAPPS HELIOS detection system, consisting primarily of a glass-fiber based spectrometer. The output pulses at 387 nm with a 150 fs pulse and a 1 kHz repetition rate were used as pump pulses. They were obtained by amplifying and frequency doubling the 775 nm seeding pulses of the Er^{3+}-doped glass fiber oscillator in a regenerative chirped-pulse titanium–sapphire amplifier and with the frequency doubling BBO crystal in the nonlinear optical amplifier (NOPA), respectively. All samples were pumped at excitation densities between 1.14×10^9 and 1.90×10^9 W/cm^2. The samples consisting of 1 mg of bare AuNC dispersed in 0.5 ml of absolute ethanol were irradiated in quartz cuvettes with a thickness of 2 mm. A fraction of the fundamental was simultaneously passed through a sapphire plate (3 mm) to generate the fs white-light continuum between 400 and 1400 nm. The chirp between 400 and 750 nm was approximately 350 fs. Transient absorption spectra of the bare AuNC in ethanol were taken at delay times between -0.5 ps and 810 ps. They were recorded in the visible region between 420 and 750 nm.

4. Results and discussions

4.1 Synthesis of bare AuNC

Here a simple one-pot synthesis method was employed to synthesize sub-nanometer sized AuNC. N, N’-dimethylformamide (DMF) was used as a solvent as well as a weakly reducing agent. It is already known from other reports[24,25] that DMF is able to act as a mild reducing agent at high temperature. In particular, the addition of a gold salt solution into a pre-heated DMF was here observed to perform as a redox reaction that predominantly yielded AuNC and a little or no formation of larger gold nanoparticles and bulk metals as by-products.

The complete mechanism of the reduction reaction is not well understood. In many previous reports[24,25], it was believed that, during the process, dimethylformamide (DMF) oxidizes to carbamic acid which in turn at high temperature can easily decompose to dimethyl amine with the evolution of carbon dioxide gas.

$$\mathrm{HCONMe_2 + Au\,(III) + H_2O \rightarrow 2Au^0 + Me_2NCOOH + 2H^+} \qquad (2)$$

$$\mathrm{Me_2NCOOH \rightarrow CO_2\uparrow + Me_2NH} \qquad (3)$$

The overall progress of the reduction reaction can be monitored observing the colour change during heating. The initially yellow gold salt solution was changed to a colourless solution after half an hour of refluxing which is assumed to be due to the formation of Au(I) in the middle of the reduction process. Finally after 5 h of refluxing, a light brown solution was formed which remained unchanged on further heating implying the completion of the reduction process.

Further evidence for the formation of luminescent AuNC can be obtained from the blue luminescence which was observed to emerge from the as-synthesized AuNC under UV-light (365 nm) irradiation (Figure 1). The AuNC dissolved in methanol exhibit a PL emission peak at 405 nm upon excitation at 330 nm (Figure 2). The PL of such AuNC is considered to arise from the electronic transitions between the $5d^{10}$ valence band and the $6sp^1$ conduction band of the gold atom.

Figure 3 shows the PL emission spectra of the AuNC that were synthesized at different refluxing times. Apparently the PL emission intensity increases with rising refluxing time, and the intensity reaches a maximum after 5 h of refluxing. On further heating, almost no change in the PL emission intensity was observed which confirms the completion of the reduction reaction.

DMF can only act as a mild reducing agent at high temperature. In contrast, at low temperature, the same reaction will yield large gold nanoparticles that exhibit surface plasmon resonance absorption instead of PL emission. This implies that the formation of AuNC requires a sufficiently high temperature, in order to activate the reducing ability of DMF to reduce metallic gold ions into non-metallic luminescent AuNC. Figure 4 shows the PL emission spectra of the products synthesized at three different refluxing temperatures that are 145°C, 100°C and 70°C, respectively. AuNC synthesized at 100°C exhibit a very low-intensity PL emission, whereas the AuNC synthesized at 70°C show no PL emission at all.

The UV-Vis absorption spectra (Figure 5) of the as-synthesized AuNC do not contain any peak at 324 nm as being characteristic for Au(III) ions which suggests the complete reduction of Au(III) into Au(0). The absence of any surface plasmon resonance peak, which appears in the range of 520-570 nm for gold nanoparticles in the absorption spectra, indicates that the reaction predominantly produces AuNC with sizes less than 2 nm. The absorption increases strongly towards shorter wavelengths around 400 nm due to interband transitions. A broad absorption band can be observed around 300-350 nm which is a finger-print band for few atoms sub-nanometer sized AuNC (Au_4–Au_{10}). The absence of plasmon absorption band in case of sub-nanometer sized AuNC was previously explained in terms of electron-surface scattering phenomenon[27,28]. The absence of the localised surface plasmon resonance (LSPR) band in small AuNC is also supported by the recent theoretical work on monolayer-protected AuNC carried out by Häkkinen and co-workers[29]. In fact, they showed by performing *ab initio* calculations how the collective electronic oscillation may change when the gold core of the experimentally observed thiolate-stabilized gold cluster grows from 1.5 to 2.0 nm. This theoretical study is of particular importance as it demonstrates a threshold size for the emergence of LSPR in these monolayer-protected AuNC. Almost no changes of the UV-Vis absorption spectra of the as-prepared bare AuNC were observed after 3 months of storage which indicates the great stability of the AuNC. Moreover, no alteration of the spectral features of their PL emission as well as no change of the UV-Vis absorption spectra was observed upon addition of a reducing agent such as $NaBH_4$ or an oxidizing agent like H_2O_2. These experimental results prove both, the high stability of the as-prepared AuNC and the absence of any Au ion in the solution.

The electronic structure and the oxidation state of the as-synthesized bare AuNC were examined upon performing XPS measurements. Figure 6 shows the Au(4f) core-level photoemission spectrum of the freeze-dried AuNC. The Au($4f_{7/2}$) binding-energy peak of the resulting AuNC (84.8 eV) is located between that of the Au(0) film (84 eV) and those of the Au(I) species (86.0 eV). This result further indicates that the reaction product mainly consists of AuNC. The dependence of the Au-4f binding energy on the nature of the surrounding ligands was previously reported[30,31,32]. A detailed peak-shape analysis of thiolate-passivated Au nanoparticles carried out by Tanaka and co-workers showed that Au($4f_{7/2}$) peaks are indeed composed of two components, one with lower binding energy originates from inner Au atoms and the other with relatively higher binding energy arises from surface Au atoms linked to thiol molecules[30]. The $4f_{7/2}$ binding energy of the surface Au atoms is generally higher in energy, since electron donation from surface Au atoms to the thiolate ligand occurs (initial-state effect). In the present study, the Au($4f_{7/2}$) core level binding energy in the cluster is slightly higher than that of the Au($4f_{7/2}$) binding energy value in an Au(0) film. This increase of the binding energy value is due to the small size of the cluster, a phenomenon explained in terms of the "final-state effect", where a coulombic attractive interaction with the photocreated holes lowers the kinetic energy of the outgoing photoelectrons.

The PL emission lifetime measurements of the as-synthesized AuNC were performed by detecting their PL emission at 405 nm upon laser excitation at 295 nm. The PL emission decay curve was simulated employing a convolution of the apparatus response and a bi-exponential decay function f(t) with $f(t) = a_1 \times \exp(-t/\tau_1) + a_2 \times \exp(-t/\tau_2)$ (Figure 7). The predominant long lifetime 3.2 ns (65 %) can be associated with the PL emission of the small sized AuNC, whereas the shorter decay time 0.8 ns (35 %) is assigned to charge-transfer states. Obviously, the AuNC exhibit PL emission that decays on the ns time scale, which is in contrast to non-emitting AuNPs[33].

The as-synthesized bare AuNC were further examined by HRTEM. Unfortunately no nanocluster with regular shapes were resolved. This observation is explained with the sub-nanometer size of the AuNC prepared in the absence of any stabilizing ligands and the limitation of lateral resolution of the used TEM. This finding is in good agreement with formerly published results[34,35].

Using fs transient absorption spectroscopy the ultrafast photo-induced electron transfer and excited state dynamics of the AuNC were investigated. The transient absorption of the AuNPs and AuNC was previously studied[36-38]. The time evolution of the transient absorption spectra of the excited-state relaxation dynamics of bare AuNC following an excitation at 387 nm is depicted in Figure 8. The excitation energy density and the time resolution used for the measurement were 1.5×10^9 W/cm^2 and 180 fs, respectively. The spectra exhibit a broad photo-induced excited state absorption signature between 400 nm and 700 nm. The observed positive transient absorption peaking around 510 nm is in sharp contrast to the transient absorption spectra of larger gold nanoparticles, where the transient absorption spectra represent superposition of a broad absorption interband component with the bleach due to plasmon resonance.

Figure 9 depicts a representative kinetic trace (detected at 530 nm) which reflects the temporal behaviour of all kinetic traces monitored between 400 and 700 nm. The kinetic traces were analyzed performing simulations with a bi-exponential function that is deconvoluted with a 240 fs Gaussian function representing the apparatus response. The kinetic traces are unambiguously characteristic for molecule-like cluster. In all kinetic traces, the bi-exponential decay dynamics comprises a fast (sub-picoseconds) and a slower (picoseconds) component. The sub-picosecond decay process presumably arose from electron-electron scattering, whereas the picosecond relaxation dynamics (4.1 ps) may be ascribed to radiationless processes such as internal conversion (IC) or intersystem crossing (ISC) which involve either promoting-mode coupling between the electronic ground and excited states or spin-orbit coupling among electronic states with different spin multiplicities.

4.2 Termination of the bare AuNC

The bare AuNC were terminated with 1-dodecanethiol (DT). Since 1-dodecanethiol contains an end-standing thiol group, this ligand binds via a covalent S-Au bond. The covalent ligand binding was performed by stirring a methanolic solution of the bare AuNC with 1-dodecanethiol in the dark. After approximately 24 h of stirring, the thiol-terminated AuNC were aged for another 24 h. Due to their small sizes AuNC have a high diffusion velocity in liquids so that inter-cluster atomic exchange processes may occur. This implies that aging processes in solutions such as Ostwald ripening may result into changes of the cluster size distribution. The observed changes of the average cluster size, surface morphology and optical properties can be monitored by optical and microscopy techniques. Here we observed that during the aging process DT-terminated AuNC grew to larger AuNC which altered the optical properties. A solvent-selective precipitation followed by ultra-centrifugation was employed to separate the larger nanocluster from the smaller ones in solution. The AuNC in the precipitate exhibited very intense red PL emission, while the rest of the solution showed blue PL under UV-light (365 nm) irradiation (Figure 10).

The blue-luminescent DT-terminated AuNC exhibited a PL emission maximum around 412 nm when excited at 330 nm, whereas the red-luminescent DT-terminated AuNC showed a PL emission peaking at 665 upon excitation at 370 nm (Figure 11). The PL emission maximum of the bare AuNC is slightly red shifted (from 405 nm to 412 nm) upon ligand attachment. The PL of the AuNC is assumed to originate from electronic transition between filled 5d band and 6sp conduction band of the gold atom. As the size of the AuNC increases, the energy gap between the discrete states in each band decreases. This leads to a red-shift of the PL emission relative to that emerging from smaller AuNC. The PL quantum yield of the blue- and red-luminescent DT-terminated AuNC were determined using quinine sulphate and rhodamine B as fluorescence standard, and the obtained values are 8.2 % and 6.7 % for the blue- and red-luminescent DT-terminated AuNC, respectively. Both, the blue- and red-luminescent DT-terminated AuNC show great chemical stability in acid and basic media. To examine the colloidal stability of these cluster, their PL emission spectrum was measured in solution at different pH values (Figure 12). Almost the same PL intensity of the blue and red DT-terminated AuNC was observed under all solvent conditions suggesting the high chemical stability of the DT-terminated AuNC in acidic and basic environment.

To further confirm the ligand binding to the gold core, FTIR measurements of the DT-terminated AuNC before aging was performed in the attenuated total reflection mode (ATR mode). The FTIR spectra of the DT-terminated AuNC and pure DT are presented in Figure 13. Most of the characteristic vibrational bands of the DT-terminated AuNC resemble those of pure DT which prove that DT is indeed a part of the cluster. Both, the DT-terminated AuNC and pure DT exhibit sharp bands at 2923 cm^{-1} and 2850 cm^{-1} which can be assigned to the asymmetric and symmetric methylene stretching modes respectively. Two bands at 2954 cm^{-1} and 2872 cm^{-1} are also present in the spectrum of the DT-terminated AuNC. These vibrational peaks are attributed to the asymmetric and symmetric stretching modes of the methyl group, respectively. The vibrational peaks in the range of 1000-1500 cm^{-1} are assigned to the C-H bending, wagging and C-C stretching vibration modes. The bands at 663 cm^{-1} and 722 cm^{-1} in the FTIR spectrum are attributed to the C-S stretching vibration of the thiol ligand. The pure 1-DT exhibits S-H stretching vibrational modes appearing at around 2557 cm^{-1}. As expected, subsequently to its reaction with bare AuNC the S-H bond stretching vibrational band completely disappears which indicates the formation of the S-Au bond. The absence of the S-H stretching vibration peak is marked by a red circle (see Figure 13).

In general, bare AuNC without any surface passivated ligands are too small to be visible in TEM. However, upon surface stabilization the sizes of the AuNC increase a bit, so that they become visible under high-resolution transmission electron microscopy (HRTEM) recorded at an accelerating voltage of 300 kV. The HRTEM images of the blue- and red-luminescent DT-terminated AuNC are depicted in Figure 14. The blue-luminescent DT-terminated AuNC are smaller than 1 nm and cannot be laterally resolved. Some of the nanocluster are marked by arrows in the HRTEM image (Figure 14C). However, the red-luminescent DT-terminated AuNC were isolated on the grid with a definite spherical shape. These red-luminescent DT-terminated AuNC show high monodispersity and the average size of these spherical particles was estimated to be 1.3 ± 0.2 nm.

Similar to bare AuNC, the time evolution of the PL emission for blue- and red-luminescent DT-terminated AuNC also includes two exponential components as shown in Figure 15. The fast and slow components have lifetimes of 0.7 ns (39 %) and 4.3 ns (61 %) for the blue-luminescent DT-terminated AuNC whereas the red-luminescent DT-terminated AuNC have lifetimes of 1.25 ns (33 %) and 5.3 ns (67 %), respectively. The observed longer lifetimes of both kinds of AuNC are in good agreement with already published results[27,28] and can be attributed to singlet transitions between low-lying d bands and excited sp bands.

5. Conclusion

In summary, we explored the mild reducing ability of N, N’-dimethylformamide (DMF) for the synthesis of luminescent AuNC. The synthesis does not require any external surfactant or protecting ligands. The AuNC are very small in size (< 1 nm) and show molecule-like features in their UV-Vis absorption spectra. The PL lifetime was found to be on the ns time scale. In addition, the fs transient absorption spectroscopy study indicates the presence of two excited-state lifetimes among which the fast sub-picosecond relaxation times at all wavelengths are assumed to originate from electron-electron scattering and the picosecond lifetimes are attributed to originate either from internal conversion or from intersystem crossing. In order to stabilize bare AuNC, 1-dodecanethiol (DT) was used as the protecting ligand. The ligand conjugation with the cluster was confirmed by FTIR spectroscopy. Moreover, the DT-terminated AuNC on further long time aging were observed to grow to larger-sized AuNC. The larger DT-terminated AuNC can be easily separated from the smaller ones employing a solvent-induced precipitation followed by ultra-centrifugation technique. Smaller DT-terminated AuNC with sizes smaller than 1 nm show blue PL emission, whereas the larger DT-terminated AuNC with an average size of about 1.3 nm exhibit prominent red PL emission. Both, the blue and red DT-terminated AuNC exhibit PL lifetimes on ns time scale.

6. Acknowledgements

Support of the Deutsche Forschungsgemeinschaft (GRK 1161/2) is gratefully acknowledged.

7. References

1. L. Li, Q. Guo, J. Li, W. Yan, C. Leng, H. Tang, Q. Lu, B. Tan, *J. Mater. Chem. B*, 2013, 1, 3999.
2. J. Zheng, P. R. Nicovich and R. M. Dickson, *Annu. Rev. Phys. Chem*., 2007, 58, 409.
3. X. Wu, X. He, K. Wang, C. Xie, B. Zhou and Z. Qing, *Nanoscale*, 2010, 2, 2244.
4. C. B. Murray, D.J. Norris and M. G. Bawendi, *J. Am. Chem. Soc*.,1993, 115, 8706.
5. W. C. W. Chan and S. Nie, *Science*, 1998, 281, 2016.
6. H. Tsunoyama, N. Ichikuni, H. Sakurai and T. Tsukuda, *J. Am. Chem. Soc.*, 2009, 131, 70.
7. T. Zhou, M. Rong, Z. Cai, C. James Yang and X. Chen, *Nanoscale*, 2012, 4, 4103.
8. N. Makarava, A. Parfenov and I. V. Baskakov, *Biophys. J.*, 2005, 89, 572.
9. T. H. Lee, J. I. Gonzalez, J. Zheng and R. M. Dickson, *Acc. Chem. Res*., 2005, 38, 534.
10. M. Scolari, A. Mews, N. Fu, A. Myalitsin, T. Assmus, K. Balasubramanian, M. Burghard, and K. Kern, *J. Phys. Chem. C*, 2008, 112, 391.
11. Mathias Brust, Merryl Walker, Donald Bethell, David J. Schiffrin and Robin Whyman., *J. Chem. Soc., Chem. Commun*., 1994, 801-802.
12. Shichibu, Y.; Negishi, Y.; Tsukuda, T.; Teranishi, T. *J. Am. Chem. Soc,* 2005, 127 (39), 13464-13465.
13. Wu, Z.; Suhan, J.; Jin, R. *J. Mater. Chem,* 2009*,* 19, 622.
14. Schaaff, T. G.; Whetten, R. L. *J. Phys. Chem. B.* 2000, 104, 2630.
15. Qian, H.; Zhu, M.; Andersen, U. N.; Jin, R. *J. Phys. Chem.* A, 2009, 113 (16) 4281–4284.

16. Levi-Kalisman, Y.; Jadzinsky, P. D.; Kalisman, N.; Tsunoyama, H.; Tsukuda, T.; Bushnell, D. A.; Kornberg, R. D., *J. Am. Chem. Soc*. 2011, 133 (9), 2976– 2982.
17. Qian, H.; Jin, R. *Chem. Mater*., 2011, 23 (8), 2209–2217.
18. Tiziano Dainese; Sabrina Antonello, Jose A. Gascon, Fangfang Pan; Neranjan.V. Perera; Marco Ruzzi; Alfonso Venzo; Alfonso Zoleo; Kari Rissanen and Flavio Maran; *ACS Nano*, 2014, *8* (4), pp 3904–3912.
19. Pal, N. K; Kryschi, C; *Phys. Chem. Chem. Phys*., 2015, 17, 1957
20. Zheng and R. M. Dickson, *J. Am. Chem. Soc.*, 2002, 124, 13982.
21. Pal, N. K; Kryschi. C; *Journal of Molecular Catalysis A: Chemical* 404 (2015) 27-35.
22. J. T. Petty, J. Zheng, N. V. Hud and R. M. Dickson, *J Am. Chem. Soc.,* 2004, 126, 5207.
23. L. Shang and S. J. Dong, *Chem. Commun.*, 2008, 1088.
24. I. Pastoriza-Santos and L. M. Liz-Marzán, *Langmuir*, 1999, 15, 948.
25. X. Liu, C. Li, J. Xu, J. Lu, M. Zhu, Y. Guo, S. Cui, H. Liu, S. Wang and Y. Li, *J. Phys. Chem. C*, 2008, 112, 10778.
26. Yabu, H., *Chem. Commun*., 2011, 47, 1196-1197
27. Kreibig, U., and von Fragstein, C., 1969, *Z. Phys*., 224, 307.
28. Kreibig. U., 1970, *Z.Phys*., 234, 307.
29. Sami Malola, Lauri Lehtovaara, Jussi Enkovaara, and Hannu Häkkinen., *ACS Nano*, 7 (11), 2013, 10263-10270.
30. Akinori Tanaka, Yuitsu Takeda, Masaki Imamura, and Shigeru Sato., *Phys. Rev.* B 68, 195415, 2003.
31. Henrik Grönbeck and Michael Odelius., *Phys. Rev. B* 82, 085416, 2010.
32. A. Chaudhuri, T. J. Lerotholi, D. C. Jackson, and D. P. Woodruff., *Phys. Rev. Lett.,* 102, 126101 (2009).
33. K. V. Mrudula, T. Udaya Bhaskara Rao and T. Pradeep*, J. Mater. Chem*., 2009, 19, 4335.
34. Duan, H., Nie, S., *J. Am. Chem. Soc*. 2007, 129, 2412-2413.
35. Jin, R., Egusa, S., Scherer, N. F., *J. Am. Chem. Soc*. 2004, 126, 9900-9901.
36. M. Farrag, M. Thämer, M. Tschurl, T. Bürgi and U. Heiz, *J. Phys. Chem. C,* 2012, 116, 8034.
37. Zhou, C.; Sun, C.; Yu, M.; Qin, Y.; Wang, J.; Kim, M.; Zheng, J. *J. Phys. Chem. C*, 2010, 114, 7727.
38. Hong, Y.; Lam, J. W. Y.; Tang, B. Z. *Chem. Soc. Rev.* 2011, 40, 5361.

8. Figures

Figure 1:

Photographs of the as-synthesized bare AuNC under ambient light exposure (left) and under UV light irradiation at 364 nm (right).

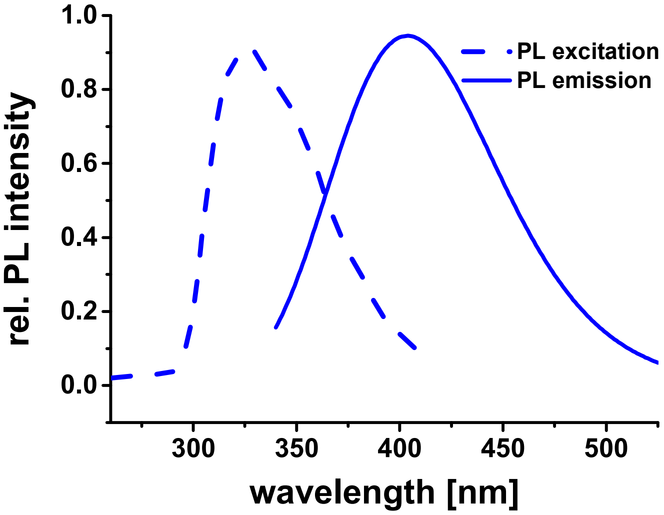

Figure 2:

PL excitation (blue dash line) and emission (blue solid line, excited at 330 nm) spectra of bare AuNC.

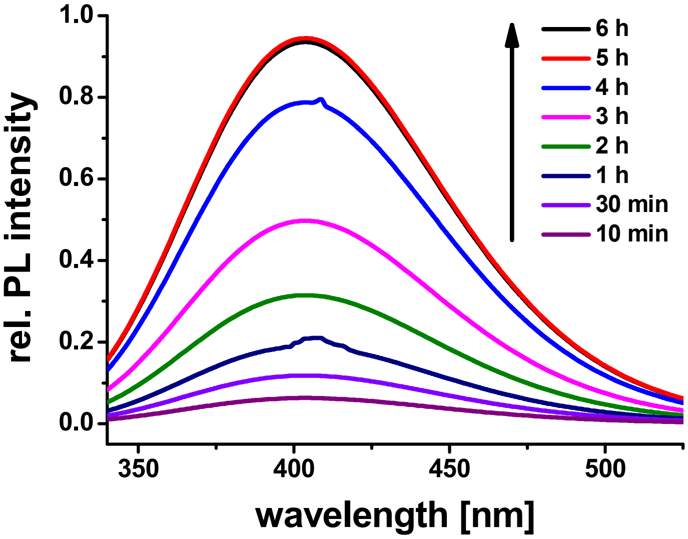

Figure 3:

PL emission spectra of bare AuNC that were synthesized at different refluxing times (excited at 330 nm).

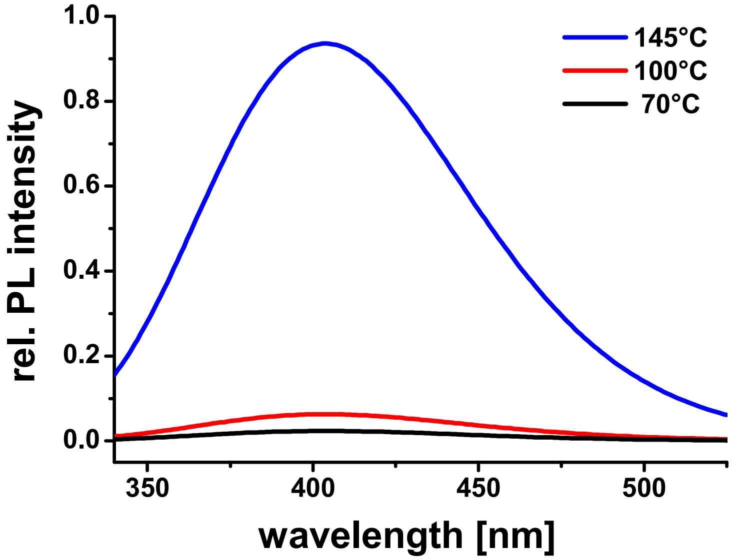

Figure 4:

PL emission spectra of bare AuNC synthesized at different refluxing temperatures: 145°C (blue solid line); 100°C (red solid line), and 70°C (black solid line).

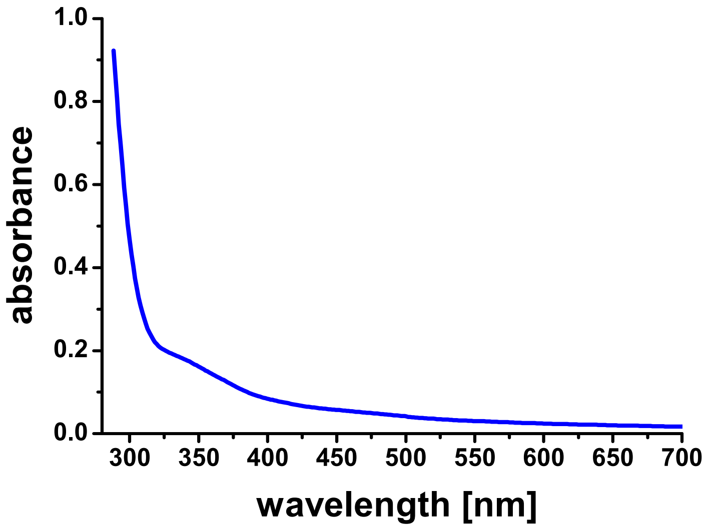

Figure 5:

The UV-Vis absorption spectrum of the as-synthesized bare AuNC.

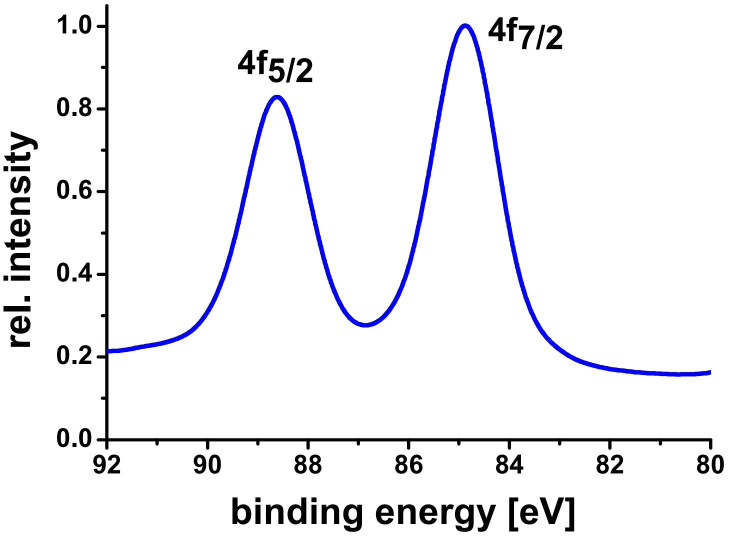

Figure 6:

Au(4f) XPS spectrum of the bare AuNC.

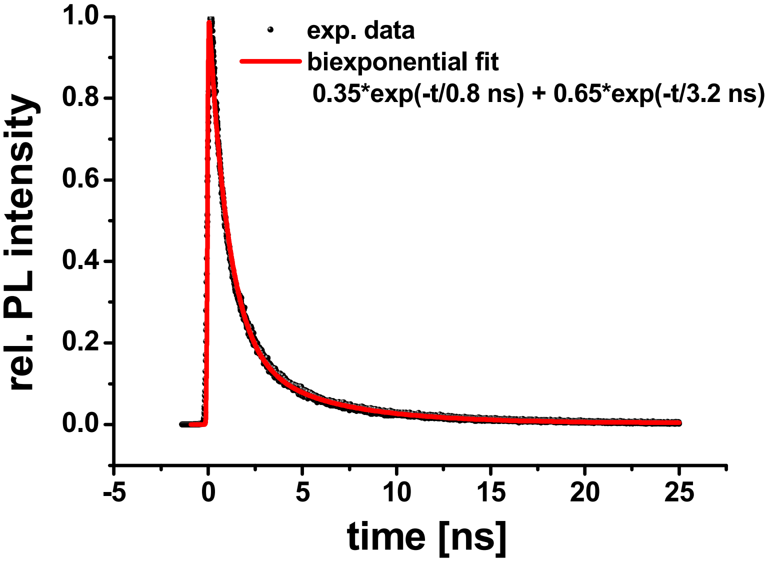

Figure 7:

The PL emission decay of the bare AuNC detected at 405 nm and excited at 295 nm. The black dots are the experimental data, whereas the solid line (red) is the best fit.

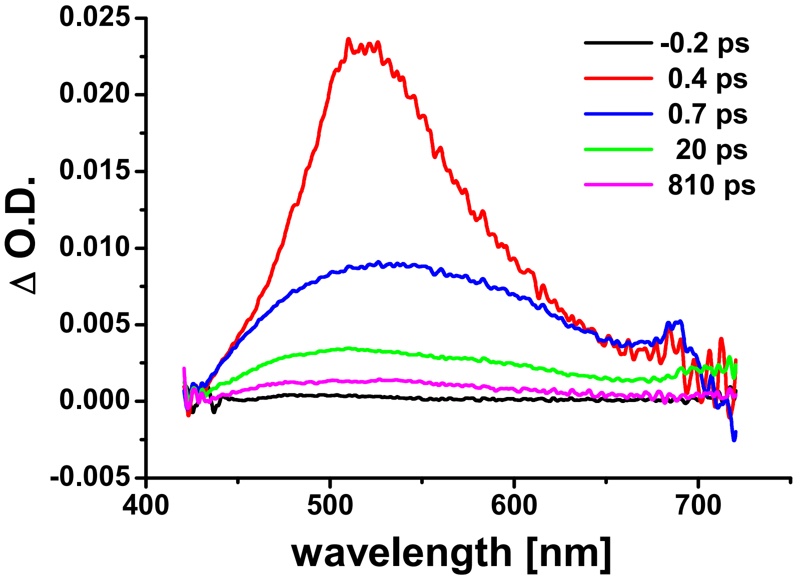

Figure 8:

Temporal evolution of the fs transient absorption spectra of the bare AuNC.

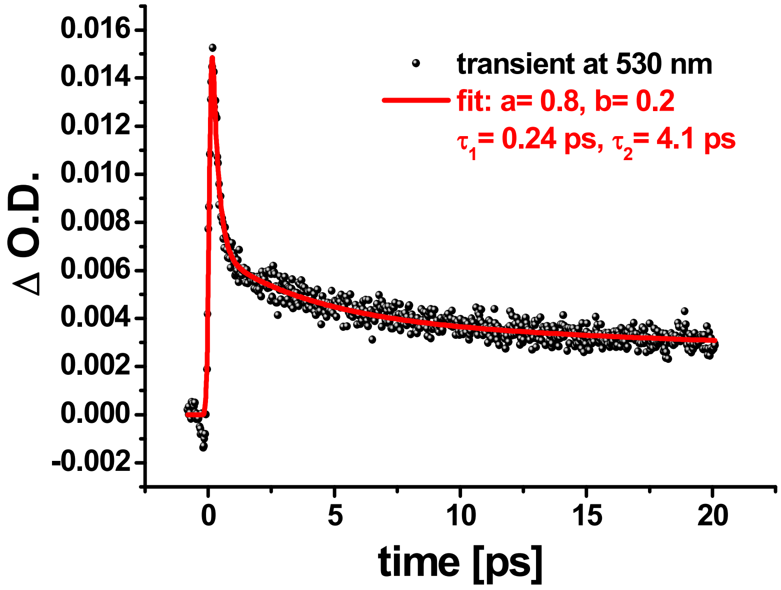

Figure 9:

Short time behaviour of the kinetic trace detected at 530 nm. The black dots are the experimental data, whereas the solid line (red) is the best fit.

Figure 10:

Photographs of blue (left) and red luminescent (right) DT-terminated AuNC under UV (365 nm) light exposure.

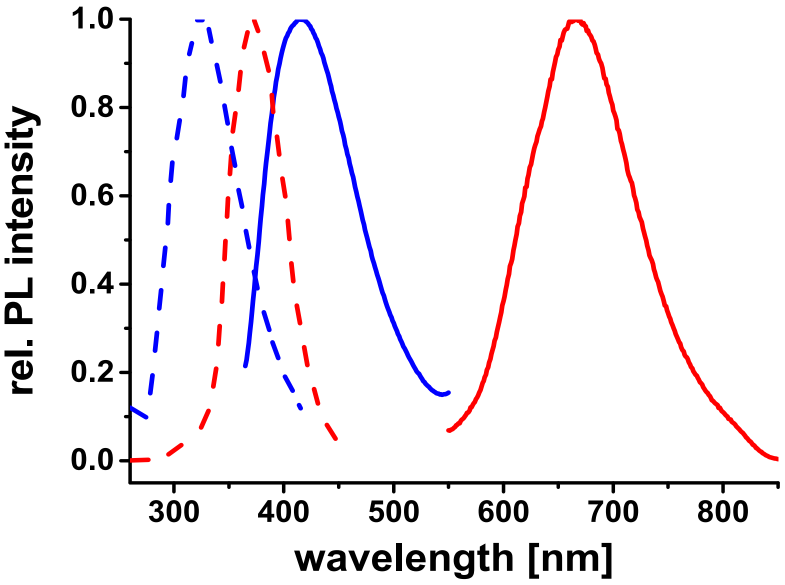

Figure 11:

PL excitation spectra of the blue (blue dashed line) and red (red dashed line) luminescent DT-terminated AuNC, whereas the PL emission spectra of the blue and red luminescent DT-terminated AuNC are drawn with blue and red solid lines, respectively.

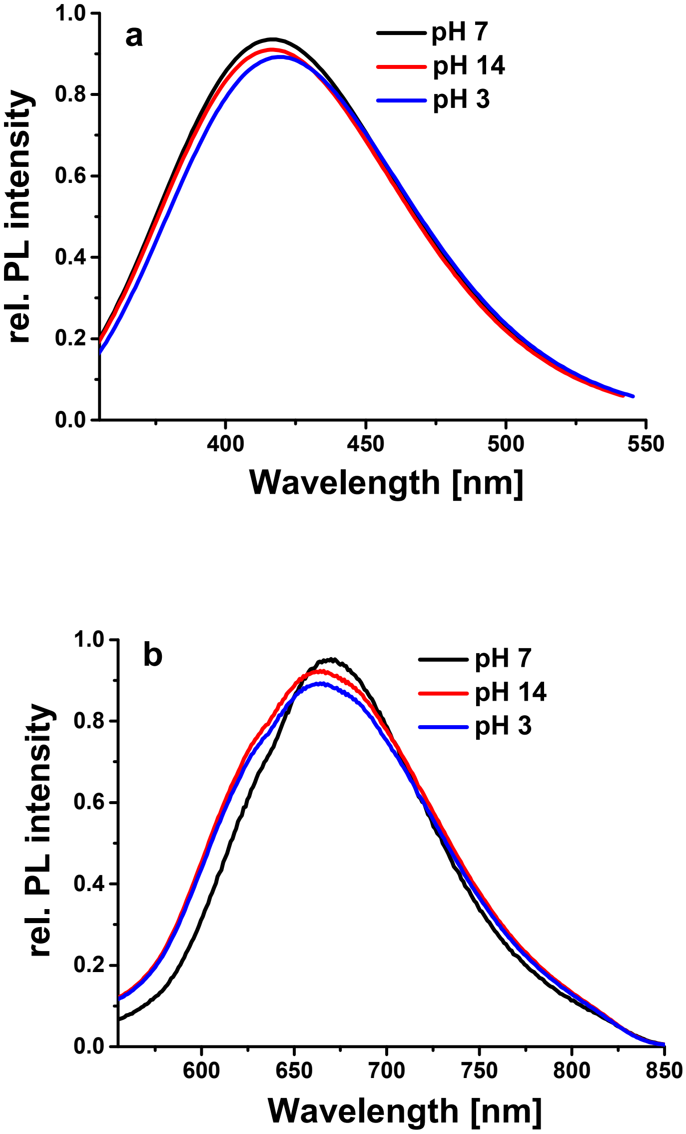

Figure 12:

PL emission spectra of blue (a) and red luminescent (b) DT-terminated AuNC in solution at pH values of 3, 7, and 14, respectively.

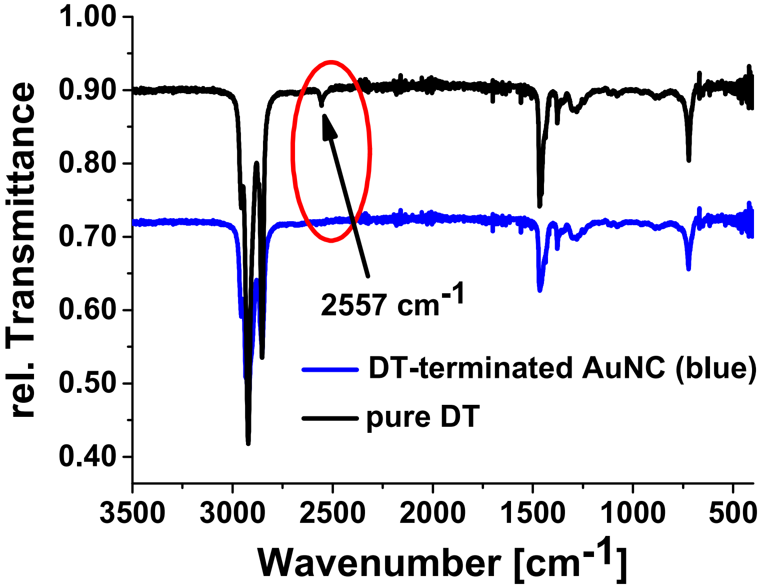

Figure 13:

FTIR-ATR spectra of pure DT (black solid line) and the blue luminescent DT-terminated AuNC (blue solid line).

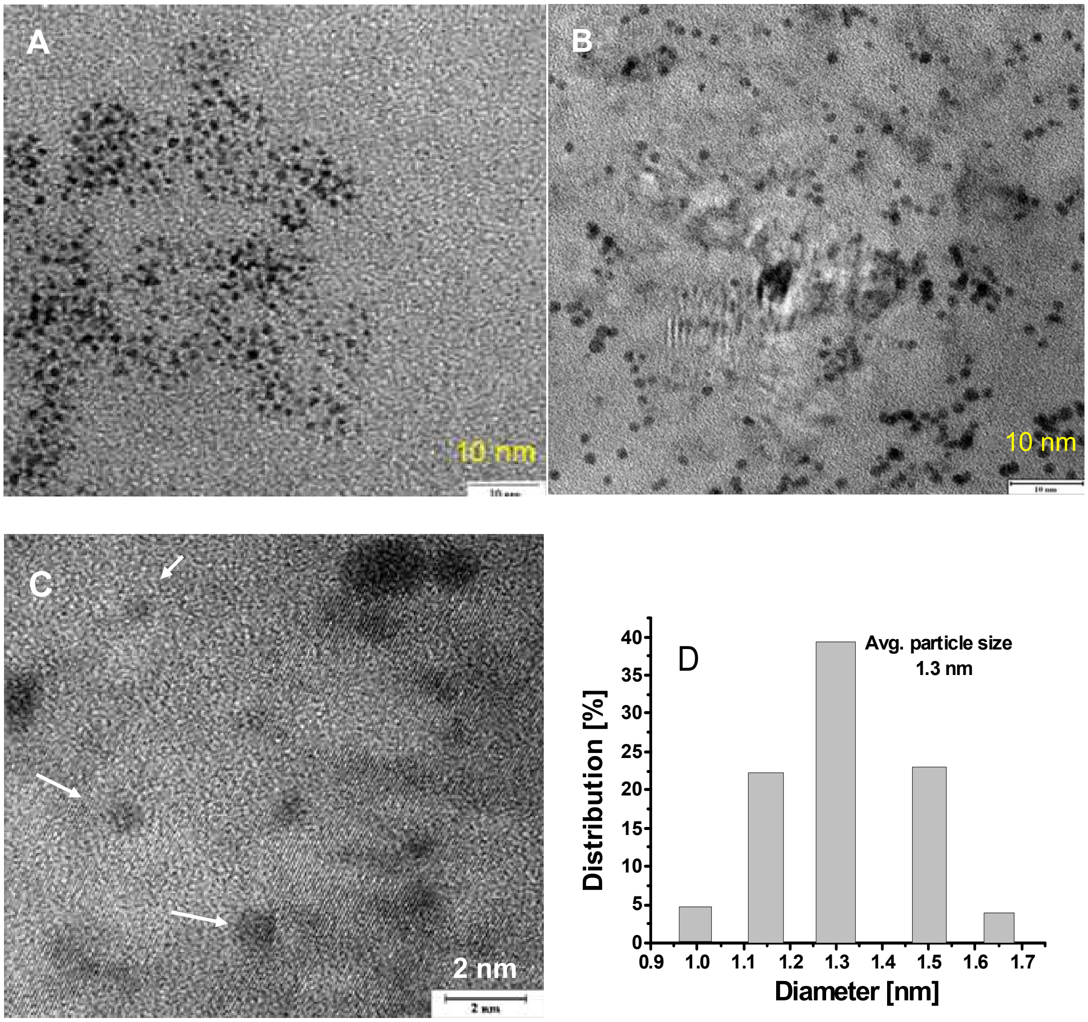

Figure 13:

HRTEM images of the blue (A, C)) and red luminescent (B) DT-terminated AuNC. A histogram of the size distribution of the red-luminescent DT-terminated AuNC is shown (D).

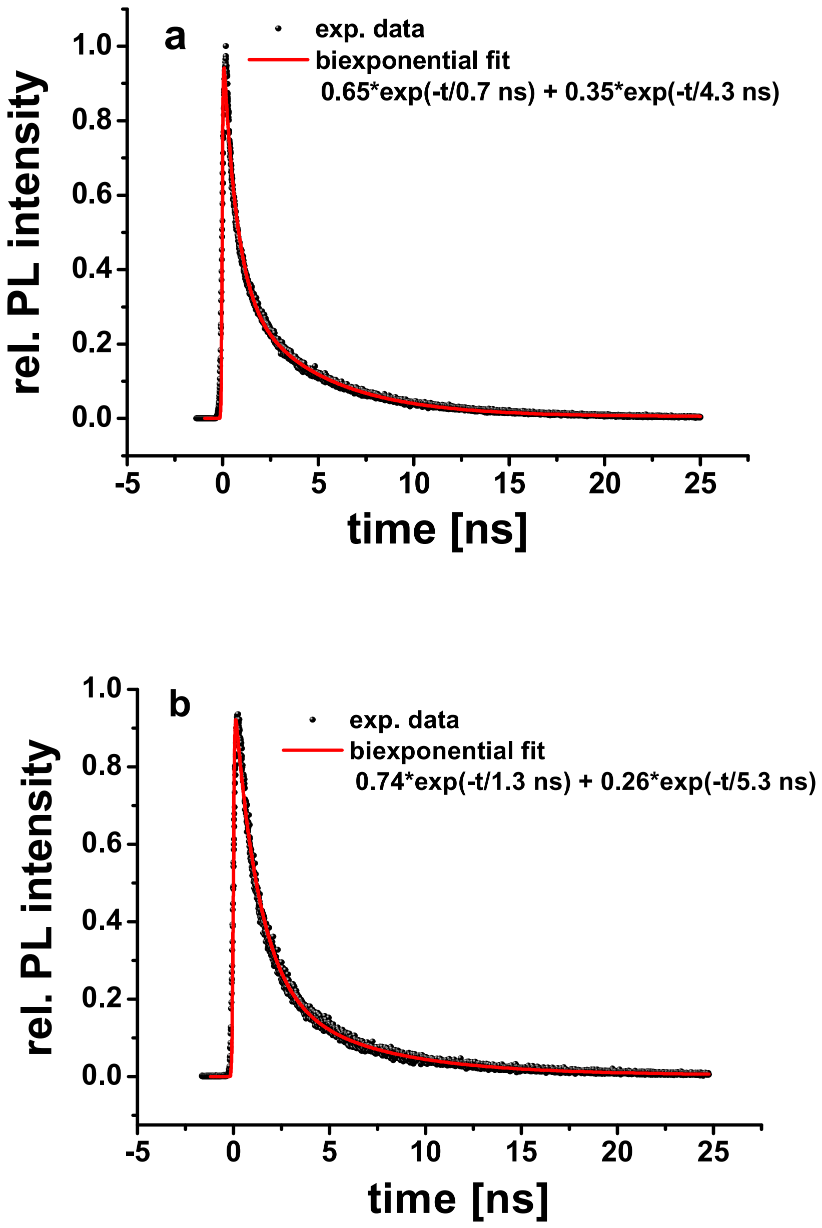

Figure 14:

PL emission decay profile of the blue (a: detected at 420 nm) and red luminescent (b: detected at 660 nm) DT-terminated AuNC (the black dots are the experimental data whereas the solid red line is the best fit).